Wide-angle invisible dielectric metasurface driven by transverse Kerker scattering

Xia Zhang [*] and A. Louise Bradley [†]
School of Physics, CRANN and AMBER, Trinity College Dublin, Dublin, Ireland

(Received 12 January 2021; revised 22 April 2021; accepted 23 April 2021; published 17 May 2021)

Interference is the cornerstone of Huygens source design for reshaping and controlling scattering patterns. The conventional underpinning principle, such as for the Kerker effect, is the interference of electric and magnetic dipole and quadrupole modes. Here a route to realize transverse Kerker scattering through employing only the interference between the electric dipole and magnetic quadrupole is demonstrated. The proposed approach is numerically validated in an ultrathin Silicon square nanoplate metasurface, and is further verified by multipole decomposition. The metasurface is shown to be invisible for near-infrared wavelengths and with an enhanced electric field in the region of the nanoparticle. Additionally, we develop further the proposed approach with practical implementation for invisibility applications by exploring the effects of the aspect ratio of the square plate nanoresonator, the interparticle separation, and the presence of a substrate. Further it is demonstrated that invisibility can be observed at oblique incidence up to 60° for a transverse magnetic plane wave. The results are relevant for Huygens metasurface design for perfect reflectors, invisibility, and devices for harmonic generation manipulation.

DOI: 10.1103/PhysRevB.103.195419

I. INTRODUCTION

In 1983, Kerker *et al.* theoretically revealed the possibility of asymmetric scattering by a magnetodielectric particle [1]. Suppressed backward scattering and near-zero forward scattering are known as the first Kerker condition and the second Kerker condition, respectively [2,3]. The principle underpinning such asymmetric scattering patterns is the interference of electric dipole (ED) and magnetic dipole (MD) resonances, which are provided by the subwavelength particle, called a Mie resonator. High-index dielectric resonators outperform plasmonic counterparts due to the higher intrinsic ohmic losses associated with the latter at optical frequencies [4,5]. Additionally, tailored by geometry, the dielectric resonator can have overlapping ED and MD resonances and provide a platform for light manipulation [6–10].

Arranging the resonators periodically in a planar geometry constitutes a Huygens metasurface under the illumination of an incident electromagnetic (EM) wave [11,12]. Each resonator behaves as the secondary source, collectively defining the outgoing beam direction [13–15]. Conceptually similar to Kerker-type scattering of a single nanoresonator, a Mie-type resonant Huygens metasurface exhibits near-unity efficiency functionalities such as perfect reflection and/or perfect transmission under normal [4,16–19] and oblique light wave incidence [20,21]. Since first reported three decades ago, the Kerker effect has been the cornerstone for exotic scattering pattern reshaping employing the coherent interplay of multipolar modes, including the only recently proposed transverse scattering in dielectric resonators [22–26]. It is a fascinating phenomenon, arising due to the simultaneous fulfillment of the first and second Kerker conditions. The traveling EM wave remains unperturbed for the lossless case, including amplitude and phase. However, remarkably different than a piece of transparent glass, the resonator has a concentrated EM field in the transverse plane. Rather than scattering forward or backward relative to the incident light propagation direction, the scatter, a single resonator, or a metasurface scatters the light only in the transverse plane. In contrast to most Huygens sources employing the interplay of only the ED and MD, the coherent contributions from available higher EM modes, the electric quadrupole (EQ), and magnetic quadrupole (MQ) play a pivotal role in transverse scattering. Upon inspection of the Green's tensor components of all multipole moments contributing to far-field scattering [27–29], it is seen that it is fundamentally impossible to realize symmetric scattering through the only interplay of ED and MD modes. The scattered electric field generated by ED or MQ displays an even parity in the plane of incidence while that of the EQ or MD display an odd parity. However, it is theoretically feasible that the transverse scattering pattern can be formed via the interplay of only the ED with the MQ or the MD with the EQ.

In sharp contrast to the work presented in Ref. [24], which fulfills the generalized amplitude and phase conditions of ED, MD, EQ, and MQ, here in this work we propose a different route to realize transverse scattering using the ED and MQ modes only. It could also be theoretically realized by the interplay of MD and EQ, which was proposed in Ref. [25] and shown in a proof-of-concept demonstration using core-shell SiO2@InSb and Si@InSb in a one-dimensional (1D) metalattice geometry in the Terahertz range. Our proposed method enables the realization of metasurface invisibility in a facile extremely thin Si square nanoplate metasurface, which is more practically feasible and offers technically easier

[*] xzhang@tcd.ie
[†] bradlel@tcd.ie

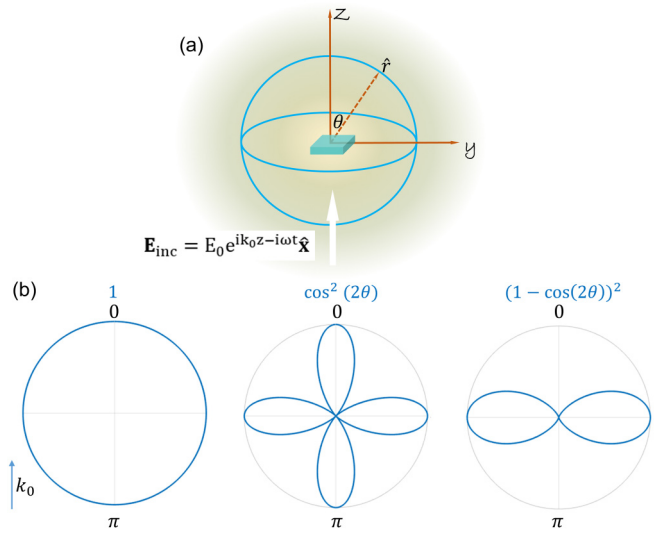

FIG. 1. (a) Schematic graph of a single stand-alone square nanoplate embedded in air. k_0 is the wave vector in air. The color background is only for better visibility. (b) The polar angular weighting factor [Eq. (2)] of the ED, MQ, and coherent sum of both when the phase differs by π in the x–z plane. A normally incident plane wave illuminates the sample from below. The incident wave is polarized along x direction and propagates along z direction.

integration into devices than core shell-type structures. Additionally, the invisibility can be tuned to a particular angle for perfect transparency. Furthermore, the proposed structure can be realized for operation in the visible and near-infrared ranges and paves the way for applications for high-efficiency nonlinear nanophotonics for second harmonic generation [30,31].

Therefore, in this work, we will first explore the principle underpinning the scattered electric field parity within a single nanoparticle case in spherical coordinates and a metasurface case in Cartesian coordinates. The conditions for perfect transverse scattering, which has an even parity with strictly no scattering in the forward and backward directions, are generalized. Additionally, we realize the transverse Kerker scattering in the extremely thin dielectric metasurface, which shows dominant ED and MQ modes with negligible MD and EQ modes. The transverse Kerker scattering is validated by numerical simulations including the scattering pattern and electric field map. For practical applications, the dependence of the interplay between the ED and MQ on the aspect ratio of the resonator, the interparticle separation, the substrate, and the angle of incidence are thoroughly studied. Our study will inspire new metasurface design and practical applications of invisible or transparent metasurfaces.

II. THEORY

We assume a stand-alone arbitrary subwavelength particle in air, the schematic can be seen in Fig. 1(a). The incident light travels along the z axis and is polarized along the x axis, expressed as $\mathbf{E}_{inc} = E_0 e^{ik_0 z - i\omega t}\hat{\mathbf{x}}$, where k_0 is the free-space wave number and $\hat{\mathbf{x}}$ is the unit vector along x axis. The total scattered electric field along all directions considering up to quadrupole modes is defined as [24,32]

$$\mathbf{E}_{sca} = \frac{k_0^2 e^{i\mathbf{k}\cdot\mathbf{r}-i\omega t}}{4\pi r\epsilon_0}\Big([\mathbf{n}\times[\mathbf{p}\times\mathbf{n}]] + \frac{1}{c}[\mathbf{m}\times\mathbf{n}] + \frac{ik_0}{6}[\mathbf{n}\times[\mathbf{n}\times(\mathbf{Q}\cdot\mathbf{n})]] + \frac{ik_0}{2c}[\mathbf{n}\times(\mathbf{M}\cdot\mathbf{n})]\Big), \quad (1)$$

where $\mathbf{r}$ is the coordinate vector and its origin is placed at the center of nanoparticle. $\mathbf{n}$ is the unit vector pointing from the origin to any coordinate position. ϵ_0 is the vacuum permittivity. $\mathbf{p}$, $\mathbf{m}$, $\mathbf{Q}$, and $\mathbf{M}$ are the ED moment, MD moment, EQ moment, and MQ moment, respectively. The expression of multipole modes is taken from Ref. [33] and the details are shown in Appendix A. In the spherical coordinate, the differential scattering cross section in the plane perpendicular to the polarization, or y–z plane as seen in Fig. 1(a) as a function of the polarizabilities is expressed as

$$\frac{d\sigma}{d\Omega}(\theta) = \left[\frac{\boldsymbol{\alpha_p}}{\epsilon_0} + \boldsymbol{\alpha_m}\cos\theta + \frac{k_0^2\boldsymbol{\alpha_Q}}{12\epsilon_0}\cos\theta + \frac{k_0^2}{4}\boldsymbol{\alpha_M}\cos(2\theta)\right]^2, \quad (2)$$

where $\boldsymbol{\alpha_p}$, $\boldsymbol{\alpha_m}$, $\boldsymbol{\alpha_Q}$, and $\boldsymbol{\alpha_M}$ are the polarizability of ED, MD, EQ, and MQ, respectively. θ is the polar angle in spherical coordinates as seen in Fig. 1. $\frac{d\sigma}{d\Omega}(\theta = 0)$ corresponds to the forward scattering along the z direction and $\frac{d\sigma}{d\Omega}(\theta = \pi)$ corresponds to the backward scattering along the $-z$ direction.

As mentioned earlier, in the plane of incidence, the scattered electric field of the ED or MQ displays an even parity while the scattered field of the MD or EQ displays an odd parity [34]. Transverse scattering, which is simultaneously zero forward and zero backward scattering, $\frac{d\sigma}{d\Omega}(\theta = 0) = \frac{d\sigma}{d\Omega}(\theta = \pi) = 0$, indicates a fundamental even parity. According to Eq. (2), the scattering pattern manifests an even parity only for $\boldsymbol{\alpha_m} = 0$ and $\boldsymbol{\alpha_Q} = 0$. Under these circumstances, transverse scattering can be achieved while satisfying two prerequisites. The first prerequisite is $\boldsymbol{\alpha_p} = -\epsilon_0 k_0^2 \boldsymbol{\alpha_M}/4$, under which condition the ED scattering destructively interferes with MQ scattering. The other prerequisite is that the polar angle weighting factor of polarizability also displays a transverse angular pattern in the plane of incidence. The polar angle weighting factors for the ED, MQ, and the destructive interference $[1-\cos(2\theta)]^2$ are shown in the bottom panel of Fig. 1, demonstrating the fulfillment of the second prerequisite.

Next we consider the more practical scenario of a metasurface in air. The backward scattering is interpreted as the reflection coefficient r. The transmission coefficient t contains the forward scattering and the incident wave contribution. Under the illumination with a plane wave $\mathbf{E}_{inc} = E_0 e^{ik_0 z - i\omega t}\mathbf{x}$, r and t in Cartesian coordinates can be expressed as [29]

$$r = \frac{ik_0}{2E_0 A\epsilon_0}\left(\mathbf{p}_x - \frac{1}{c}\mathbf{m}_y + \frac{ik_0}{6}\mathbf{Q}_{xz} - \frac{ik_0}{2c}\mathbf{M}_{yz}\right),$$
$$t = 1 + \frac{ik_0}{2E_0 A\epsilon_0}\left(\mathbf{p}_x + \frac{1}{c}\mathbf{m}_y - \frac{ik_0}{6}\mathbf{Q}_{xz} - \frac{ik_0}{2c}\mathbf{M}_{yz}\right), \quad (3)$$

where A is the area of a unit cell of the metasurface. Multipolar modes are multipolar EM waves in origin with their inherent amplitude and phase along forward and backward

directions. $\mathbf{p}_x$ refers to the total electric dipole, which includes the toroidal dipole contribution.

Similar to the single nanoparticle case, the multipolar EM wave displays a strictly even parity only if $|i\mathbf{m}_y/c|$ and $|k_0\mathbf{Q}_{xz}/6|$ are negligible compared with ED and MQ contributions. Then Eq. (3) can be rewritten as $r = \frac{ik_0}{2E_0A\epsilon_0}(\mathbf{p}_x - \frac{ik_0}{2c}\mathbf{M}_{yz})$ and $t = 1 + \frac{ik_0}{2E_0A\epsilon_0}(\mathbf{p}_x - \frac{ik_0}{2c}\mathbf{M}_{yz})$. When the condition $r = 0$ is fulfilled, then $t = 1$, both forward and backward scattering from the metasurface disappear and transverse Kerker scattering is achieved. For the lossless case, the amplitude of incident light wave remains unperturbed. The metasurface behaves as nonexistent or transparent, referred to as the lattice invisibility effect or extraordinary transmission elsewhere [29]. According to Eq. (3), with negligible MD and EQ contribution, the generalized amplitude and phase conditions for transverse scattering are

$$|i\mathbf{m}_y/c| \approx 0,\ |k_0\mathbf{Q}_{xz}/6| \approx 0,$$
$$|i\mathbf{p}_x| = \left|\frac{k_0}{2c}\mathbf{M}_{yz}\right|,$$
$$\varphi(i\mathbf{p}_x) = \varphi\left(\frac{k_0}{2c}\mathbf{M}_{yz}\right) \pm (2n+1)\pi. \quad (4)$$

Additionally, perfect reflection can be achieved if $t = 0$, where the scattered EM waves destructively interfere with the transmitted incident electric field, in which case

$$r = \frac{ik_0}{2E_0A\epsilon_0}\left(\mathbf{p}_x - \frac{ik_0}{2c}\mathbf{M}_{yz}\right) = -1, \quad (5)$$

where for the lossless case, the incident wave is fully reflected and metasurface behaves as a perfect mirror and is referred to as a Huygens reflector.

III. METASURFACE INVISIBILITY FOR LIGHT AT NORMAL INCIDENCE

Next we test the feasibility of the concept in a single nanoparticle or a metasurface with negligible MD and EQ contributions. An extremely thin high refractive index metasurface, such as a Si square nanoplate metasurface, meets the prerequisites of negligible MD and EQ contributions. The much lower aspect ratio is crucial to suppress the MD and EQ contributions and is demonstrated by multipole decomposition following Ref. [33]. The conditions for negligible MD and EQ are determined by sweeping the geometrical aspect ratio, which is the ratio of the height H, to the edge length of the square nanoplate L. The aspect ratio is varied from 0.04 to 0.4, where the Mie-like mode is the scope of this study rather than Fabry-Pérot-like modes within the metasurface [35–37]. Regarding the dependence of the amplitudes of the multipolar modes on the height of the nanoplate or aspect ratio, see Fig. S1 of the Supplemental Material [38].

Additionally, the period along the x, D_x, and y directions D_y are also swept separately to explore the evolution of the ED and MQ modes, with details shown in Fig. S2 of the Supplemental Material [38]. The wavelength-dependent real and imaginary parts of the refractive index and permittivity are obtained from fitting the experimental data in Ref. [39]. All numerical simulations are performed using the Lumerical finite-difference time domain (FDTD) tool. Periodic boundary

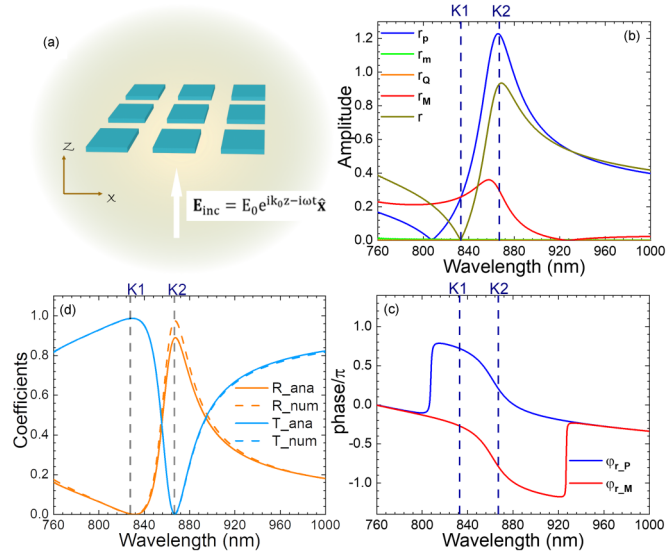

FIG. 2. (a) Schematic of the periodic Si square nanoplate metasurface embedded in air. The color background is shown only for better visibility of the nanostructure. The period is $D_x = D_y =$ 750 nm, with L = 460 nm and H = 40 nm. A normally incident plane wave interacts with the metasurface. The incident wave, $\mathbf{E}_{inc} = E_0 e^{i(k_0 z - \omega t)}\hat{\mathbf{x}}$, is polarized along x direction and propagates along z direction. (b) Amplitude of the multipole moments from Eq. (3), including $r_\mathbf{p}$, $r_\mathbf{m}$, $r_\mathbf{Q}$, $r_\mathbf{M}$ and r. (c) Phase profile of $r_\mathbf{p}$ and $r_\mathbf{M}$. (d) Numerically simulated (_num) and semi-analytically calculated (_ana) reflection (R) and transmission (T) coefficients. Two wavelengths selected for detailed analysis are indicated by the vertical dashed lines, at $K1$ 833 nm, $K2$ 867 nm, respectively.

conditions are applied on four sides of the unit cell to simulate the electric field distribution of an infinite two-dimensional array of particles. The electric field distribution within one unit cell takes account of the electric field distribution of each resonator and the coupling between resonators.

Here we present as an example the results for the Si square nanoplate metasurface in air which has the edge length, $L =$ 460 nm, height $H = 40$ nm, and period $D_x = D_y = 750$ nm. The schematic representation can be seen in Fig. 2(a). An infinite periodic array of Si square nanoplates is illuminated by a normally incident plane wave $\mathbf{E}_{inc} = E_0 e^{i(k_0 z - \omega t)}\hat{\mathbf{x}}$, which propagates along the z direction and is polarized along the x direction.

According to the standard expansion method in Ref. [33], we consider the decomposition of the multipolar modes up to quadrupole modes by integrating the electric field over the square nanoplate volume. The decomposed multipole moments contributing to the reflection in Eq. (3) are denoted as $r_\mathbf{p} = ik_0\mathbf{p}_x/(2E_0A\epsilon_0)$, $r_\mathbf{m} = -ik_0\mathbf{m}_y/(2cE_0A\epsilon_0)$, $r_\mathbf{Q} = -k_0^2\mathbf{Q}_{xz}/(12E_0A\epsilon_0)$, and $r_\mathbf{M} = k_0^2\mathbf{M}_{yz}/(4cE_0A\epsilon_0)$. The corresponding amplitude and phase are presented in Figs. 2(b) and 2(c), respectively. It is clear in Fig. 2(b) that the amplitude of the MD and EQ is negligible. The dominant multipole moments are the ED and MQ. The semi-analytically calculated and the directly numerically calculated reflection coefficient $R = |r|^2$ and transmission coefficient $T = |t|^2$, following Eq. (3), are presented in Fig. 2(d), and are found to be in excellent agreement. This demonstrates that the multipole

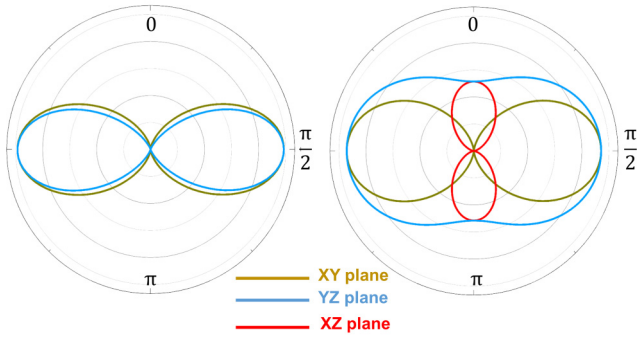

FIG. 3. The simulated far-field scattering power profile for one single resonator in the array, $|E|^2$ at $K1$ 833 nm and $K2$ 867 nm, respectively. The angle 0 indicates the incident light propagation direction or the forward direction while π indicates the backward direction for x–z and y–z planes. In x–y plane, x direction points toward $\pi/2$.

decomposition up to quadrupole modes is sufficient and consideration of higher-order modes is not required.

Special attention is paid to the wavelengths at 833 nm and 867 nm, denoted as $K1$ and $K2$, respectively, and shown by dashed lines in Figs. 2(b), 2(c) and 2(d). At $K1$, ED and MQ share the same amplitude and differ only by a phase of $\approx \pi$. According to Eq. (3), $r = r_{\mathbf{p}} + r_{\mathbf{M}}$, the reflection coefficient $R = |r|^2 = |r_{\mathbf{p}}|^2 + |r_{\mathbf{M}}|^2 + 2|r_{\mathbf{p}}||r_{\mathbf{M}}|\cos(\varphi_{r_{\mathbf{p}}} - \varphi_{r_{\mathbf{M}}}) \approx 0$. This explains the zero reflection coefficient at 833 nm. The ED component $r_{\mathbf{p}}$ destructively interferes with the MQ component $r_{\mathbf{M}}$. As mentioned earlier, in this situation, $t = 1$. The transmitted light has only the contribution from the incident wave without the scattering signal from the resonators in metasurface. This corresponds well with the near unity transmission at $K1$ as shown in Fig. 2(d). Transverse Kerker scattering is expected at $K1$ according to generalized conditions in Eq. (4). Upon a closer look at $K2$ 867 nm, ED and MQ do not have equal amplitude but they differ in phase by π. There is still destructive interference between ED and MQ according to the amplitude of $r_{\mathbf{p}}$, $r_{\mathbf{M}}$, and r shown in Fig. 2(b) as $r < r_p$. However, ED and MQ cannot completely cancel each other at this wavelength due to their unequal amplitudes. It is expected that the scattering pattern at $K2$ is symmetric in the forward and backward directions, displaying an even parity due to the inherent even parity of the ED and MQ modes.

To confirm our expectations and also to provide an intuitive picture, the far-field scattering intensity profile of one metasurface unit cell is calculated and presented in Fig. 3 for both $K1$ 833 nm and $K2$ 867 nm. It is clear that the far-field scattering intensity pattern is symmetric in the x–y, y–z, and x–z planes, which is determined by the even parity of the ED and MQ modes. Notably, it is zero over the x–z plane at $K1 = 833$ nm, including both the forward and backward directions, which manifests the transverse scattering pattern. At $K2$ 867 nm, it is clear that the far-field scattering intensity pattern is symmetric but forward and backward scattering still occur. The ED destructively interferes with MQ, but full destructive interference is not achieved due to the unequal amplitudes. The real part of the electric field at the $K1$ and $K2$ wavelengths are presented in Fig. 4 in the x–z plane. As expected at $K1$ 833 nm, the incident wave propagates along the z direction and transmits through the metasurface almost without perturbation. The metasurface is rendered invisible, the so-called lattice invisibility [25]. At $K2$ 867 nm, as expected by Eq. (5), the incident wave, expressed as the absolute value of the amplitude ratio $|E_x/E_0|$, is reflected back and the metasurface behaves as a perfect mirror. Note that as stated earlier, both forward and backward scattering remain at $K2$ 867 nm, the coherent sum of ED and MQ destructively interferes with the transmitted incident EM wave, which results in near-zero transmission and near-unity reflection. This mechanism underpins the principle of the Si metasurface-based perfect mirror.

With a view to practical applications, a metasurface with dominant ED and MQ on a substrate with low refractive index, such as refractive index 1.45, which matches the refractive index of glass, quartz, and polymers, is now considered. Introducing the substrate will shift the spectral positions of resonant modes compared with a metasurface embedded in air medium, as can be seen Figs. 5(b) and 5(d). Correspondingly the wavelengths at which invisible or near-perfect transparency occurs also shift, which is clearly seen in the reflection and transmission spectra shown in Figs. 5(a) and 5(c). The invisibility wavelength for the metasurface ($L = 500$ nm, $H = 50$ nm, $D_x = D_y = 600$ nm) shifts from 900 nm in air to 955 nm for the metasurface sitting on the substrate. Additionally, the substrate modifies the electric field distribution within the metasurface at the invisibility wavelength, as can be seen from Figs. 5(e) and 5(f). A larger electric field

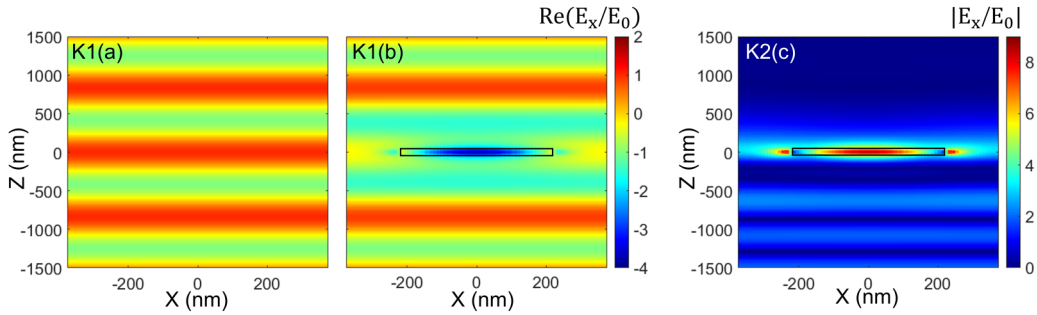

FIG. 4. Real part of the normalized scattered electric field, $\mathrm{Re}(E_x/E_0)$, in the x–z plane (a) without and (b) with the square plate at $K1 = 833$ nm. The square nanoplate resonator in one metasurface unit cell is shown by the black box. (c) The absolute value of the normalized scattered electric field, $|E_x/E_0|$ in the x–z plane at $K2 = 867$ nm.

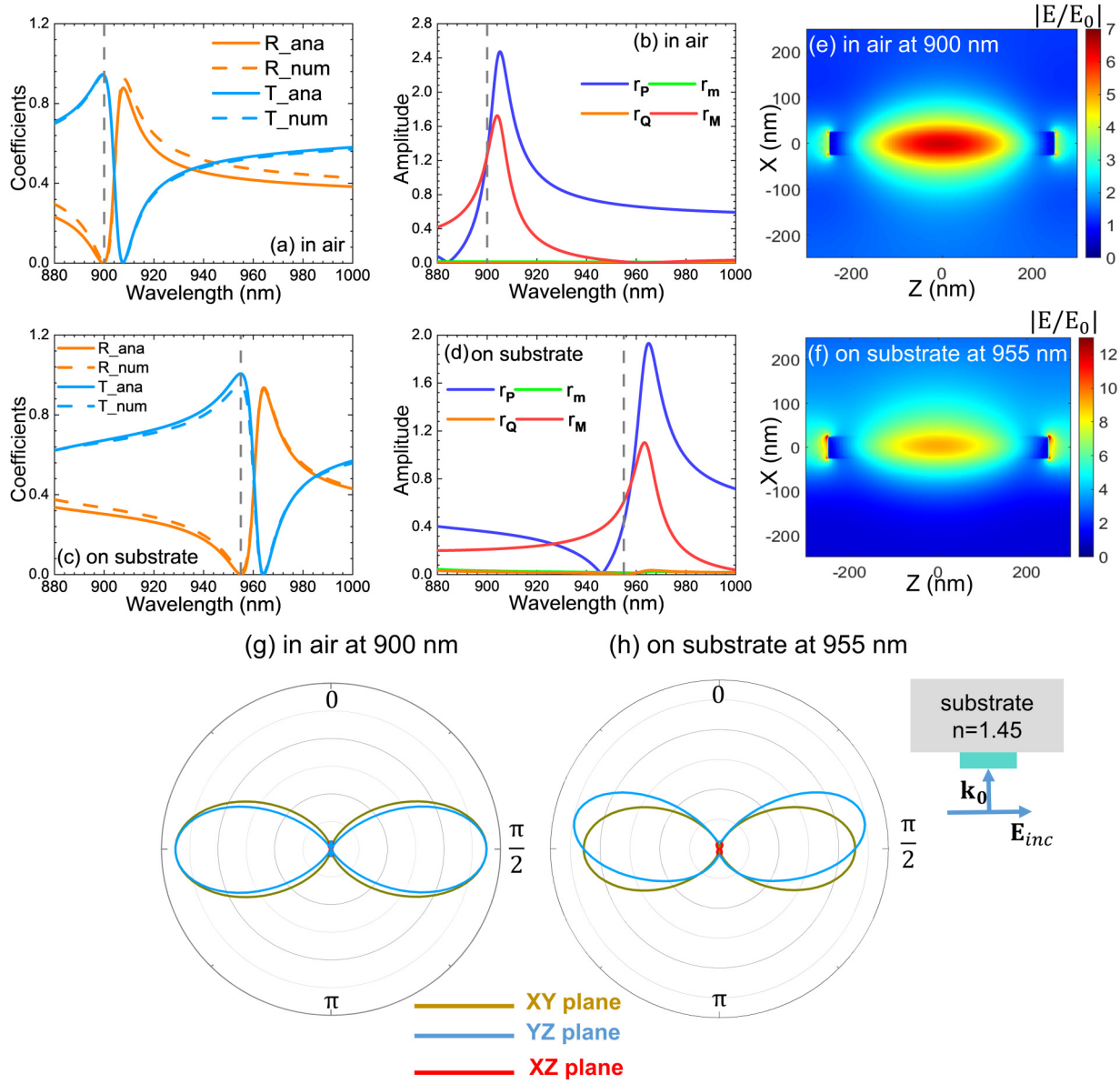

FIG. 5. (a, c) Numerically simulated (_num) and semi-analytically (_ana) calculated reflection (R) and transmission (T) for the Si square nanoplates ($L = 500$ nm, $H = 50$ nm, $D_x = D_y = 600$ nm) in air and on a substrate, where the substrate has the refractive index 1.45. (b, d) The calculated amplitude of multipolar modes of the metasurface in air and on the substrate. The inspected wavelengths are shown as gray dash lines. (e, f) The electric field distribution in the x–z plane and (g, h) the simulated far-field scattered power profile for one single resonator in the array at 900 nm in air and at 955 nm on the substrate, respectively. The metasurface in air or on the substrate is illuminated by normally incident plane wave propagating upwards, as shown in the schematic in (h).

amplitude is obtained due to the presence of the substrate. For the metasurface sitting on the substrate, the amplitudes of resonant modes are calculated from the electric field distribution within the metasurface sitting on the substrate rather than that in air. The reflection and transmission spectra obtained using the semi-analytical approach, according to Eq. (3), agree well with the spectra calculated directly from the numerical simulation, as can be seen clearly from Fig. 5(c). This demonstrates that the light reflected from substrate and Fabry-Pérot multiple reflections within the ultrathin metasurface can be considered as negligible [40]. More details on the substrate effects for these ultrathin dielectric resonators can be found elsewhere [41].

Additionally, as seen in Fig. 5(g), the scattering profile at 900 nm, for the metasurface in air, shows a perfect transverse scattering pattern, where the scattering lobe is symmetric and mainly in transverse directions. However, the scattering pattern is modified due to the existence of the substrate as seen in Fig. 5(h), where an asymmetric pattern in the x–z and y–z planes is observed. There is a slight tilt of the side lobes, though it is less than has been observed in the case of employing the coherent interplay of ED, MD, EQ, and MQ to achieve transverse scattering, as reported, for example, in Ref. [24]. The approach of using only the coherent interplay of ED and MQ appears to be less affected by the substrate, with the scattering mainly confined to the transverse plane.

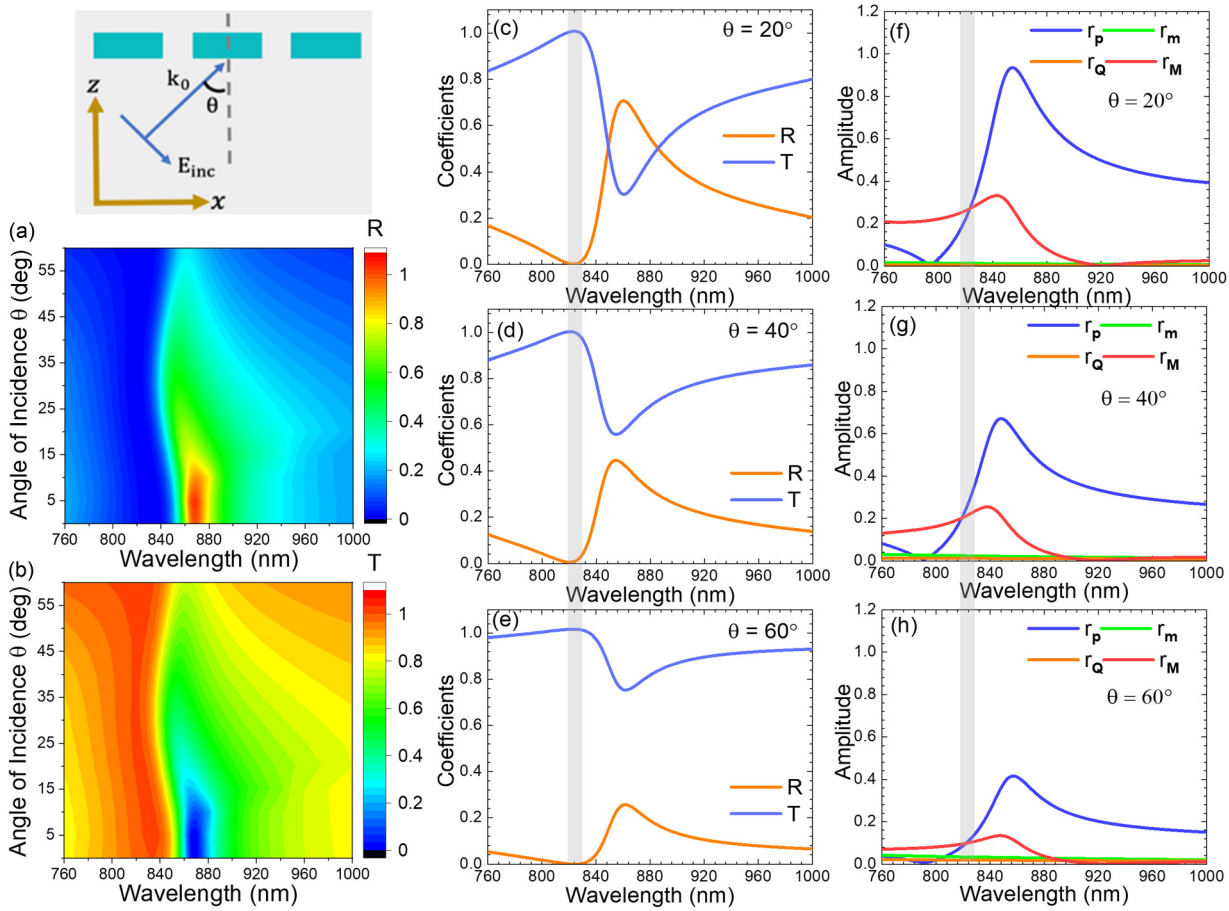

FIG. 6. The schematic showing transverse magnetic (TM) polarized oblique incidence light wave. θ is the angle between the wave vector k_0 and the z-direction, and is defined as the incident angle. (a, b) The contour plots of the numerically simulated reflection and transmission spectra for a metasurface with a TM-polarized plane wave incident at an oblique angle θ up to 60°. (c)–(e) The numerically simulated reflection and transmission spectra for the metasurface under the illumination with a TM polarized plane wave with an incident angle of $\theta = 20°$, $\theta = 40°$, and $\theta = 60°$, respectively. The shaded area illustrates the wavelength range where the metasurface is rendered nearly invisible or transparent. (f)–(h) The corresponding multipolar contributions generated by the TM plane-wave incident at angles of $\theta = 20°$, $\theta = 40°$, and $\theta = 60°$, respectively.

IV. METASURFACE INVISIBILITY WITH TM POLARIZED LIGHT AT OBLIQUE INCIDENCE

In this section, we explore how the invisibility evolves under excitation with light at oblique angles of incidence for the metasurface in air. Oblique plane-wave incidence changes the spectral positions of the resonant multipoles [37]. The transverse magnetic (TM) oblique wave incidence corresponds to a change in D_x while the transverse electric (TE) oblique wave incidence corresponds to a change in D_y. As mentioned earlier, the effect of changing lattice constant or period along x and y directions, respectively, can be found in the Supplemental Material Fig. S2 [38]. For the metasurface illuminated by a normally incident plane wave polarized along the x-axis, the spectral positions of resonant ED and MQ modes are not significantly affected by the D_x but gradually red-shift with increasing D_y. TM oblique incidence corresponds to changes of D_x [40], therefore, invisibility at a constant wavelength could be expected under oblique TM incidence, but is not possible for TE polarized light. To further explore the possibility of wide-angle invisibility, the Broadband Fixed Angle Source Technique (BFAST) is used for broadband angle-resolved simulations using Lumerical FDTD [42–45].

The contour plots of the numerically simulated angle-resolved reflection and transmission spectra can be seen in Figs. 6(a) and 6(b). It is clear that the invisibility, or transparency, still remains at oblique angle incidence although with a slight spectra shift. The wavelength range, or transparency wavelength window, is illustrated as the shaded area in Figs. 6(c), 6(d) and 6(e), where near-perfect transparency exists at all angles. To probe more the underlying physics, multipolar decomposition analysis for various angles of incidence for a TM polarized plane wave, including 20°, 40°, 60°, is undertaken and shown in Figs. 6(f), 6(g) and 6(h). With increasing angle of incidence θ, where the incident light polarization can be decomposed into z and x polarized light waves, the amplitude of the x-polarized wave becomes effectively $|E_{\text{inc}}\cos\theta|$, and therefore the amplitude of ED and MQ decrease, which are clearly seen in Figs. 6(f), 6(g) and 6(h). However, overlapping resonant modes are still achieved and the spectral position of the overlap does not shift significantly, as can be seen by the shaded area. The invisibility studied

in this work is driven by transverse Kerker scattering, or destructive interference of the ED and MQ, therefore the equal amplitude, as seen in Figs. 6(f), 6(g) and 6(h), and coherence properties of the ED and MQ guarantees the wide-angle invisibility or transparency.

V. CONCLUSION

To conclude, starting from a general description the resonant multipolar modes for a single arbitrary subwavelength nanoparticle and the properties of transverse Kerker scattering are discussed. The transverse Kerker scattering field and intensity exhibit an even parity in the forward and backward directions. The description was then extended to consider a metasurface, in which rather than employing the coherent interplay of the ED, MD, EQ, and MQ to achieve transverse scattering, only the ED and MQ multipoles are employed. The proposed route is numerically realized in an ultrathin Si square nanoplate metasurface in air and could be extended to any extremely thin arbitrary shape nanoparticle, where a low aspect ratio guarantees negligible MD and EQ contributions. It is shown that the proposed configuration is valid for a metasurface embedded in a homogeneous medium or on a substrate with low refractive index, such as polymer, glass, or quartz. Additionally, it is demonstrated that due to the extremely thin layer thickness, our proposed metasurface shows robust TM incident angle independence where the invisibility or near-perfect transparency can be achieved, although there are slight spectra position shifts. Our study can inspire new Huygens metasurface design with ultrathin nanostructures and spur further experimental investigations for perfect mirrors, perfect transmission, and other invisibility applications, as well as exploitation of the transverse scattered fields.

ACKNOWLEDGMENTS

We wish to acknowledge the support of Science Foundation Ireland (SFI) under Grant No. 16/IA/4550.

APPENDIX

The expression of multipolar modes in Cartesian coordinates is [28]

$$\begin{aligned}
\mathbf{P} &= \int \epsilon_0(\epsilon_{Si}-1)\mathbf{E}(\mathbf{r})d\mathbf{r},\\
\mathbf{T} &= \frac{-i\omega}{10c}\int \epsilon_0(\epsilon_{Si}-1)\{[\mathbf{r}\cdot\mathbf{E}(\mathbf{r})]\mathbf{r}-2\mathbf{r}^2\mathbf{E}(\mathbf{r})\}d\mathbf{r},\\
\mathbf{m} &= -\frac{i\omega}{2}\int \epsilon_0(\epsilon_{Si}-1)[\mathbf{r}\times\mathbf{E}(\mathbf{r})]d\mathbf{r},\\
\mathbf{Q} &= 3\int \epsilon_0(\epsilon_{Si}-1)\left\{\mathbf{r}\mathbf{E}(\mathbf{r})+\mathbf{E}(\mathbf{r})\mathbf{r}-\frac{2}{3}[\mathbf{r}\cdot\mathbf{E}(\mathbf{r})]\hat{U}\right\}d\mathbf{r},\\
\mathbf{M} &= \frac{\omega}{3i}\int \epsilon_0(\epsilon_{Si}-1)\{[\mathbf{r}\times\mathbf{E}(\mathbf{r})]\mathbf{r}+\mathbf{r}[\mathbf{r}\times\mathbf{E}(\mathbf{r})]\}d\mathbf{r},
\end{aligned} \tag{A1}$$

where $\mathbf{r}$ is the coordinate vector with its origin placed at the center of the square nanoplate. $\mathbf{E}(\mathbf{r})$ is the total electric field inside the nanoplate at different position. ϵ_0 is the vacuum permittivity; ϵ_{Si} is the relative dielectric permittivity of the Si particle. c is the light speed in a vacuum; $\hat{U}$ is the 3×3 unity tensor; $\mathbf{p}$, $\mathbf{T}$, $\mathbf{m}$, $\mathbf{Q}$, and $\mathbf{M}$ are the moments of ED, TD, MD, electric quadrupole (EQ), and MQ, respectively. The total electric dipole $\mathbf{p}$ is calculated as $\mathbf{p}=\mathbf{P}+ik\mathbf{T}$.

[1] M. Kerker, D.-S. Wang, and C. L. Giles, Electromagnetic scattering by magnetic spheres, JOSA **73**, 765 (1983).
[2] A. Alu and N. Engheta, How does zero forward-scattering in magnetodielectric nanoparticles comply with the optical theorem? J. Nanophotonics **4**, 041590 (2010).
[3] B. García-Cámara, J. M. Saiz, F. González, and F. Moreno, Nanoparticles with unconventional scattering properties: Size effects, Opt. Commun. **283**, 490 (2010).
[4] Y. F. Yu, A. Y. Zhu, R. Paniagua-Domínguez, Y. H. Fu, B. Luk'yanchuk, and A. I. Kuznetsov, High-transmission dielectric metasurface with 2π phase control at visible wavelengths, Laser Photonics Rev. **9**, 412 (2015).
[5] I. Staude and J. Schilling, Metamaterial-inspired silicon nanophotonics, Nat. Photonics **11**, 274 (2017).
[6] J. M. Geffrin, B. García-Cámara, R. Gómez-Medina, P. Albella, L. Froufe-Pérez, C. Eyraud, A. Litman, R. Vaillon, F. González, M. Nieto-Vesperinas, J. J. Sáenz, and F. Moreno, Magnetic and electric coherence in forward-and back-scattered electromagnetic waves by a single dielectric subwavelength sphere, Nat. Commun. **3**, 1 (2012).
[7] A. B. Evlyukhin, S. M. Novikov, U. Zywietz, R. L. Eriksen, C. Reinhardt, S. I. Bozhevolnyi, and B. N. Chichkov, Demonstration of magnetic dipole resonances of dielectric nanospheres in the visible region, Nano Lett. **12**, 3749 (2012).
[8] Y. H. Fu, A. I. Kuznetsov, A. E. Miroshnichenko, Y. F. Yu, and B. Luk'yanchuk, Directional visible light scattering by silicon nanoparticles, Nat. Commun. **4**, 1527 (2013).
[9] A. I. Kuznetsov, A. E. Miroshnichenko, M. L. Brongersma, Y. S. Kivshar, and B. Luk'yanchuk, Optically resonant dielectric nanostructures, Science **354**, aag2472 (2016).
[10] D.-H. Kwon, G. Ptitcyn, A. Díaz-Rubio, and S. A. Tretyakov, Transmission Magnitude and phase control for polarization-preserving reflectionless metasurfaces, Phys. Rev. Appl. **9**, 034005 (2018).
[11] M. Decker, I. Staude, M. Falkner, J. Dominguez, D. N. Neshev, I. Brener, T. Pertsch, and Y. S. Kivshar, High-efficiency dielectric huygens' surfaces, Adv. Opt. Mater. **3**, 813 (2015).
[12] A. M. H. Wong and G. V. Eleftheriades, Perfect Anomalous Reflection with a Bipartite Huygens' Metasurface, Phys. Rev. X **8**, 011036 (2018).
[13] C. L. Holloway, E. F. Kuester, J. A. Gordon, J. O'Hara, J. Booth, and D. R. Smith, An overview of the theory and applications of metasurfaces: The two-dimensional equivalents of metamaterials, IEEE Antennas Propag. Mag. **54**, 10 (2012).

[14] D. Lin, P. Fan, E. Hasman, and M. L. Brongersma, Dielectric gradient metasurface optical elements, Science **345**, 298 (2014).

[15] H.-T. Chen, A. J. Taylor, and N. Yu, A review of metasurfaces: physics and applications, Rep. Prog. Phys. **79**, 076401 (2016).

[16] C. Pfeiffer and A. Grbic, Metamaterial Huygens' Surfaces: Tailoring Wave Fronts with Reflectionless Sheets, Phys. Rev. Lett. **110**, 197401 (2013).

[17] M. Kim, A. M. H. Wong, and G. V. Eleftheriades, Optical Huygens' Metasurfaces with Independent Control of the Magnitude and Phase of the Local Reflection Coefficients, Phys. Rev. X **4**, 041042 (2014).

[18] I. Staude, A. E. Miroshnichenko, M. Decker, N. T. Fofang, S. Liu, E. Gonzales, J. Dominguez, T. S. Luk, D. N. Neshev, I. Brener, and Y. Kivshar, Tailoring directional scattering through magnetic and electric resonances in subwavelength silicon nanodisks, ACS nano **7**, 7824 (2013).

[19] V. E. Babicheva and A. B. Evlyukhin, Resonant lattice kerker effect in metasurfaces with electric and magnetic optical responses, Laser Photonics Rev. **11**, 1700132 (2017).

[20] D. R. Abujetas, J. A. Sanchez-Gil, and J. J. Sáenz, Generalized brewster effect in high-refractive-index nanorod-based metasurfaces, Opt. Express **26**, 31523 (2018).

[21] M. Nieto-Vesperinas, R. Gomez-Medina, and J. Saenz, Angle-suppressed scattering and optical forces on submicrometer dielectric particles, J. Opt. Soc. Am. A **28**, 54 (2011).

[22] J. Y. Lee, A. E. Miroshnichenko, and R.-K. Lee, Simultaneously nearly zero forward and nearly zero backward scattering objects, Opt. Express **26**, 30393 (2018).

[23] A. Bag, M. Neugebauer, P. Woźniak, G. Leuchs, and P. Banzer, Transverse Kerker Scattering for Angstrom Localization of Nanoparticles, Phys. Rev. Lett. **121**, 193902 (2018).

[24] H. K. Shamkhi, K. V. Baryshnikova, A. Sayanskiy, P. Kapitanova, P. D. Terekhov, P. Belov, A. Karabchevsky, A. B. Evlyukhin, Y. Kivshar, and A. S. Shalin, Transverse Scattering and Generalized Kerker Effects in All-Dielectric Mie-Resonant Metaoptics, Phys. Rev. Lett. **122**, 193905 (2019).

[25] M. Liu and C. Zhao, Lattice invisibility effect based on transverse kerker scattering in 1D metalattices, J. Phys. D: Appl. Phys. **52**, 495107 (2019).

[26] H. K. Shamkhi, A. Sayanskiy, A. C. Valero, A. S. Kupriianov, P. Kapitanova, Y. S. Kivshar, A. S. Shalin, and V. R. Tuz, Transparency and perfect absorption of all-dielectric resonant metasurfaces governed by the transverse kerker effect, Phys. Rev. Mater. **3**, 085201 (2019).

[27] A. B. Evlyukhin, C. Reinhardt, A. Seidel, B. S. Luk'yanchuk, and B. N. Chichkov, Optical response features of si-nanoparticle arrays, Phys. Rev. B **82**, 045404 (2010).

[28] A. B. Evlyukhin, T. Fischer, C. Reinhardt, and B. N. Chichkov, Optical theorem and multipole scattering of light by arbitrarily shaped nanoparticles, Phys. Rev. B **94**, 205434 (2016).

[29] P. D. Terekhov, V. E. Babicheva, K. V. Baryshnikova, A. S. Shalin, A. Karabchevsky, and A. B. Evlyukhin, Multipole analysis of dielectric metasurfaces composed of nonspherical nanoparticles and lattice invisibility effect, Phys. Rev. B **99**, 045424 (2019).

[30] H. Liu, C. Guo, G. Vampa, J. L. Zhang, T. Sarmiento, M. Xiao, P. H. Bucksbaum, J. Vučković, S. Fan, and D. A. Reis, Enhanced high-harmonic generation from an all-dielectric metasurface, Nat. Phys. **14**, 1006 (2018).

[31] K. Koshelev, S. Kruk, E. Melik-Gaykazyan, J.-H. Choi, A. Bogdanov, H.-G. Park, and Y. Kivshar, Subwavelength dielectric resonators for nonlinear nanophotonics, Science **367**, 288 (2020).

[32] J. D. Jackson, *Classical Electrodynamics* (Wiley, New York, 1999).

[33] P. D. Terekhov, K. V. Baryshnikova, Y. A. Artemyev, A. Karabchevsky, A. S. Shalin, and A. B. Evlyukhin, Multipolar response of nonspherical silicon nanoparticles in the visible and near-infrared spectral ranges, Phys. Rev. B **96**, 035443 (2017).

[34] W. Liu and Y. S. Kivshar, Generalized kerker effects in nanophotonics and meta-optics, Opt. Express **26**, 13085 (2018).

[35] M. V. Rybin, K. L. Koshelev, Z. F. Sadrieva, K. B. Samusev, A. A. Bogdanov, M. F. Limonov, and Y. S. Kivshar, High-Q Supercavity Modes in Subwavelength Dielectric Resonators, Phys. Rev. Lett. **119**, 243901 (2017).

[36] M. V. Rybin, K. B. Samusev, P. V. Kapitanova, D. S. Filonov, P. A. Belov, Y. S. Kivshar, and M. F. Limonov, Switchable invisibility of dielectric resonators, Phys. Rev. B **95**, 165119 (2017).

[37] A. A. Bogdanov, K. L. Koshelev, P. V. Kapitanova, M. V. Rybin, S. A. Gladyshev, Z. F. Sadrieva, K. B. Samusev, Y. S. Kivshar, and M. F. Limonov, Bound states in the continuum and fano resonances in the strong mode coupling regime, Adv. Photon. **1**, 016001 (2019).

[38] See Supplemental Material at http://link.aps.org/supplemental/10.1103/PhysRevB.103.195419 for more details on the dependence of the amplitudes of the multipolar modes on the height of the nanoplate or aspect ratio, as well as on the metasurface periodicity.

[39] D. E. Aspnes and A. A. Studna, Dielectric functions and optical parameters of Si, Ge, GaP, GaAs, GaSb, InP, InAs, and InSb from 1.5 to 6.0 eV, Phys. Rev. B **27**, 985 (1983).

[40] V. E. Babicheva, M. I. Petrov, K. V. Baryshnikova, and P. A. Belov, Reflection compensation mediated by electric and magnetic resonances of all-dielectric metasurfaces, J. Opt. Soc. Am. B **34**, D18 (2017).

[41] X. Zhang, J. Li, J. F. Donegan, and A. L. Bradley, Constructive and destructive interference of Kerker-type scattering in an ultrathin silicon Huygens metasurface, Phys. Rev. Mater. **4**, 125202 (2020).

[42] Y. Liang, K. Koshelev, F. Zhang, H. Lin, S. Lin, J. Wu, B. Jia, and Y. Kivshar, Bound states in the continuum in anisotropic plasmonic metasurfaces, Nano Lett. **20**, 6351 (2020).

[43] V. E. Babicheva, Lattice effect in Mie-resonant dielectric nanoparticle array under oblique light incidence, MRS Commun. **8**, 1455 (2018).

[44] H. Gao, D. Zhou, W. Cui, Z. Liu, Y. Liu, Z. Jing, and W. Peng, Ultraviolet broadband plasmonic absorber with dual visible and near-infrared narrow bands, J. Opt. Soc. Am. A **36**, 264 (2019).

[45] B. Liang, M. Bai, H. Ma, N. Ou, and J. Miao, Wideband analysis of periodic structures at oblique incidence by material independent FDTD algorithm, IEEE Trans. Antennas Propag. **62**, 354 (2013).